Research Article

Journal of PeptideScience

Received: 30 December 2009 Revised: 16 April 2010 Accepted: 16 April 2010 Published online in Wiley Interscience: 6 July 2010

(www.interscience.com) DOI 10.1002/psc.1250

Mapping interactions of gastric inhibitory polypeptide with GIPR *N*-terminus using NMR and molecular dynamics simulations

Sonali H. Tikhele,[a] Raghuvir R. S. Pissurlenkar,[a] Sudha Srivastava,[b] Anil Saran[a] and Evans C. Coutinho[a]*

Glucose-dependent insulinotropic polypeptide (gastric inhibitory polypeptide, or GIP), a 42-amino acid incretin hormone, modulates insulin secretion in a glucose-concentration-dependent manner. Its insulinotropic action is highly dependent on glucose concentration that surmounts the hypoglycemia side effects associated with current therapy. In order to develop a GIP-based anti-diabetic therapy, it is essential to establish the 3D structure of the peptide and study its interaction with the GIP receptor (GIPR) in detail. This will give an insight into the GIP-mediated insulin release process. In this article, we report the solution structure of GIP(1–42, human)NH_2 deduced by NMR and the interaction of the peptide with the *N*-terminus of GIPR using molecular modelling methods. The structure of GIP(1–42, human)NH_2 in H_2O has been investigated using 2D-NMR (DQF-COSY, TOCSY, NOESY, ^1H-^{13}C HSQC) experiments, and its conformation was built by constrained MD simulations with the NMR data as constraints. The peptide in H_2O exhibits an α-helical structure between residues Ser8 and Asn39 with some discontinuity at residues Gln29 to Asp35; the helix is bent at Gln29. This bent gives the peptide an 'L' shape that becomes more pronounced upon binding to the receptor. The interaction of GIP with the *N*-terminus of GIPR was modelled by allowing GIP to interact with the *N*-terminus of GIPR under a series of decreasing constraints in a molecular dynamics simulation, culminating with energy minimization without application of any constraints on the system. The canonical *ensemble* obtained from the simulation was subjected to a detailed energy analysis to identify the peptide–protein interaction patterns at the individual residue level. These interaction energies shed some light on the binding of GIP with the GIPR *N*-terminus in a quantitative manner.

Keywords: diabetes; glucose-dependent insulinotropic polypeptide; GIP(1–42) NH_2; GIP receptor (GIPR); 2D-NMR; G-protein-coupled receptor (GPCR); MD simulations

Introduction

Glucose-dependent insulinotropic polypeptide (GIP, also known as gastric inhibitory polypeptide) has attracted attention as a potential therapy for type 2 diabetes mellitus (T2DM) because of its glucose-dependent insulinotropic effect. GIP, a 42-amino acid residue peptide (YAEGT^{5}FISDY^{10}SIAMD^{15}KIHQQ^{20}DFVNW^{25}LLAQK^{30}GKKND^{35}WKHNI^{40}TQ) [1], is secreted by the enteroendocrine K-cells of the intestine in response to food ingestion [2]. GIP stimulates insulin secretion in a glucose-dependent manner through its interaction with a class 2 G-protein-coupled receptor (GPCR). The binding initiates signal transduction by activation of adenylate cyclase and other signal transduction pathways, ultimately leading to increased intracellular Ca^{2+} concentration and enhanced exocytosis of insulin-containing granules [3]. GIP is considered to be one of the principal factors accounting for up to 80% of the insulinotropic response to nutrient ingestion [4]. In addition to aiding glucose absorption, there are speculations of its vital role in fat absorption and metabolism [5–8].

Therapeutic use of native GIP in the treatment of T2DM is precluded due to the short half-life of GIP (approximately 7 min in healthy individuals and 5 min in patients with T2DM) [9]. This short half-life is a result of the presence of an alanine residue at position 2 which makes GIP a potential substrate for enzymatic inactivation by dipeptidyl peptidase IV (DPP-IV). DPP-IV is an aminopeptidase that cleaves dipeptides when alanine or proline is present at position 2 in the amino terminus [10]. GIP is metabolised to a truncated metabolite GIP(3–42), which is a GIP receptor (GIPR) antagonist *in vivo*. In order to circumvent this degradation, DPP-IV inhibitors are being used as a therapy for T2DM; but the effects of long-term interference on the metabolism of a plethora of other peptide substrates for DPP-IV are yet unknown. Plausibly, a more attractive approach than the use of nonspecific inhibition of DPP-IV is to design and synthesise specific GIP analogues with modifications at the cleavage site [11]. However, despite the remarkable potential for GIP analogues in the treatment of T2DM, their peptidic nature effectively rules out the option of straightforward oral administration.

Therefore in order to develop a GIP-based T2DM therapy, that is, say small molecules that mimic the actions of GIP, it is essential to establish the 3D structure of the native GIP and study its interaction

* *Correspondence to: Evans C. Coutinho, Department of Pharmaceutical Chemistry, Bombay College of Pharmacy, Kalina, Santacruz (E), Mumbai 400 098, India. E-mail: evans@bcpindia.org*

a *Department of Pharmaceutical Chemistry, Bombay College of Pharmacy, Kalina, Santacruz (E), Mumbai 400 098, India*

b *National Facility for High Field NMR, Tata Institute of Fundamental Research, Homi Bhabha Road, Navy Nagar, Colaba, Mumbai 400 005, India*

with GIPR at the atomic level. These kind of interaction studies are of great importance in understanding the function of the peptide and will shed light on the important features of ligands (peptide and/or non-peptide) necessary for tight binding to GIPR to invoke the glucose-dependent insulinotropic response. We had previously deduced the solution structure of porcine GIP(1–30) NH_2 (YAEGT[5] FISDY[10]SIAMD[15]KIRQQ[20]DFVNW[25]LLAQK[30]; GIP truncated at residue number 30, His18 in human GIP is replaced by Arg18 in porcine GIP), which is equipotent to the full-length GIP, in H_2O and DMSO-d_6 using 2D-NMR and MD simulations [12]. There are other reports of the NMR structure of the truncated (1–30) and the full-length (1–42) GIP in various solvents like H_2O and the mixture (TFE)-d_3:H_2O [13,14]. All these studies indicate the presence of some degree of α-helicity in the structure of GIP. Recently the crystal structure [15] of GIP bound to the *N*-terminus of GIPR has been published. While the study sheds light on some aspects of peptide–protein binding, a glaring absence is the electron densities of the terminal nine residues – Lys33 to Gln42. Moreover the use of methyl β-cyclodextrin for crystallization of the protein obscures finer details of the interaction with the *N*-terminal portion of GIP. This study is an attempt to fill in the missing gaps in the interaction of GIP (1–42) with the *N*-terminus of GIPR, not as a static picture but as it evolves over time.

In order to map the interactions of GIP with the *N*-terminus of GIPR that is not encumbered by any additives or crystal packing forces, it is essential that the 3D structure of GIP is established under conditions as close to the native environment as possible. NMR and X-ray crystallography are the most widely used methods for 3D structure determination of peptides and proteins. Each of these methods has inherent advantages and disadvantages. Application of NMR spectroscopy is limited to small (<40 kDa), stable, soluble proteins that do not aggregate at the high concentrations required for NMR studies. The higher dimensional NMR experiments require doubly labelled ^{13}C and ^{15}N samples. Also NMR data interpretation and assignments takes a huge amount of time. Although X-ray crystal structures are a good source of 3D structures of macromolecules with bound substrates or inhibitors revealing the binding site for the macromolecules, the dynamics of the interactions are not evident. The NMR experiments are carried out in solutions and conditions such as temperature, pH and salt concentration can be adjusted so as to closely mimic a physiological fluid. Furthermore, in addition to structure determination, NMR is capable of investigating the dynamic features of the molecular structures, as well as the structural, thermodynamic and kinetic aspects of the interactions between proteins/peptides and other solution components. In the crystal, a static or a single frame structure is seen and only one parameter set can be extracted. As a result the study of motions, especially of domain movements, is not possible. Consequently a crystal structure is inefficient in providing insights into the dynamic interactions of the receptor–ligand (peptides or small molecules) which takes place over a period of time. Also the X-ray crystal structures can be erroneous at times due to improper interpretations of the electron densities obtained at low resolution. The small size of GIP (42 amino acids) makes NMR a good choice for structure determination. Structural inputs obtained from NMR experiments when used in conjunction with molecular modelling strategies yield conformations that are consistent with the experimental data at atomic level resolution. Molecular dynamics simulation connects structure and function by providing additional information to the NMR data and gives a deeper insight into the various aspects of receptor–ligand interactions. The basic idea in molecular dynamics simulation is to allow the system to evolve in time so that the system will eventually pass through all the possible states. This enables us to study the energetics and dynamics of the interactions between the peptide and the receptor as they evolve over the entire trajectory.

In this article, we present the 3D solution structure of GIP(1–42, human)NH_2 in H_2O, as determined by NMR spectroscopy and molecular dynamics simulation and its interaction with the *N*-terminal domain of GIPR over a molecular dynamics simulation trajectory of 6 ns. The interaction has been quantified in a residue-wise manner to obtain a comprehensive analysis of the thermodynamic events involved in the binding of GIP to the *N*-terminus of the GIPR.

Methods

NMR Sample Preparation

GIP(1–42) NH_2 (human, hereafter referred to as *h*GIP) was purchased from Bachem, UK. Isotopically enriched ^2H_2O was purchased from Sigma Chemical Co., USA. 2,2-Dimethyl-2-silapentan-5-sulphonate (DSS) was from Stohler Isotope Chemicals, USA. For NMR studies, the peptide was dissolved in 95 : 5 H_2O : D_2O mixture to obtain a concentration of ~2 mM. At this concentration, no aggregation was observed for the peptide. DSS was used as an internal reference standard.

NMR Experiments

The NMR experiments were carried out on Bruker Avance 800 MHz FT-NMR spectrometer operating at a ^1H resonance frequency of 800 MHz at 298 K. Data was processed using Topspin software version 2.1.

Phase-sensitive total correlation spectroscopy (TOCSY) and double quantum filtered correlation spectroscopy (DQF-COSY) [16] experiments were carried out for the assignment of spin systems of the amino acids. Nuclear Overhauser Effect Spectroscopy (NOESY) [17] was used for connecting the spin systems of the individual amino acid residues, i.e sequential assignment. The TOCSY spectrum was acquired at 298 K with a spinlock mixing time of 80 ms, using the MLEV-17 [18] sequence. Six NOESY spectra were acquired with 64 scans at 298 K using the phase-sensitive 2D-NOESY pulse sequence. The NOESY spectra were recorded with mixing times of 50, 100, 150, 200, 250 and 300 ms to construct the NOE buildup curves. At the beginning of each experiment, 16 dummy scans were collected to allow the system to reach thermal equilibrium. The data were apodised with a sine-bell window function and zero filled to a matrix of size 4K × 2K data points prior to Fourier transformation. To determine the temperature coefficients of the NH chemical shifts, TOCSY and NOESY spectra were also recorded at temperatures of 298, 308 and 318 K. Coupling constants ($^3J_{NH\alpha}$) were extracted from a double quantum filtered COSY (DQF-COSY) spectrum that was acquired with 96 scans and digitised with 4K data points in the t_2 dimension. ^1H-^{13}C gradient heteronuclear single quantum correlation (HSQC) experiments with sensitivity enhancement were recorded with 192 scans to obtain the ^{13}C chemical shifts in both solvents.

For suppression of the water signal the powerful technique of *excitation sculpting* [19] was used in all the experiments. Chemical shifts in all the spectra were referenced internally to DSS.

Structure Calculation

^{1}H and ^{13}C chemical shifts, the patterns of intra- and inter-residue NOEs, the $^3J_{NH\alpha}$ coupling constants, temperature coefficients of the amide resonances and the chemical shift index (CSI) of the H_α resonances were used to draw inferences about the secondary structure of the peptide.

NOE intensities were determined from the NOESY spectra using the integration routine in the Topspin programme. Interproton distances were calculated from the cross-peak intensities using the following equation:

$$r_{ij} = rkl\left(\frac{I_{kl}}{I_{ij}}\right)^{1/6} \quad (1)$$

where r_{ij} and r_{kl} are the distances, and I_{ij} and I_{kl} the NOE intensities of proton pairs i,j and k,l, respectively. Interproton distances calculated from the NOEs were classified, adjusted to preset values (three ranges: 1.8–2.8 Å, 1.8–3.6 Å and 1.8–5.0 Å) and corrected for methyl, methylene and aromatic rings according to the rules formulated by Wüthrich [20]. Pseudoatom corrections were also introduced. The corrected interproton distances were used as distance restraints in an MD simulation to generate the solution structure.

Temperature coefficients of NH chemical shifts were measured from the 2D-TOCSY spectra recorded in the temperature range 298–318 K for the peptide. The $^3J_{NH\alpha}$ coupling constants were converted to the ϕ values through the modified Karplus equation [21]:

$$^3J_{NH\alpha} = 6.51\cos^2(\varphi - 60) - 1.76\cos(\varphi - 60) + 1.60 \quad (2)$$

and introduced as dihedral restraints. The dihedral, distance and chirality restraints were incorporated into a Simulated Annealing (SA) protocol involving a slow heating at 600 K followed by cooling at 300 K in steps of 10 K with a total dynamics run of 25 ps at each stage, with the *Discover* module of *InsightII* [22]. The 300 K trajectory was sampled every 1 ps to give a total of 25 structures. The CFF91 forcefield [23] potentials and partial charges were used for all atoms in the simulation. The 25 structures sampled from the 300 K MD trajectory were energy minimised by a combination of steepest descents and conjugate gradients to yield an *ensemble* of structures, from which the global minimum energy structure was taken for further simulation. This latter simulation was carried out using *Desmond* (v*2.2)* module in the Schrodinger Suite 2009 (DE Shaw Research group) [24]. The global minimum energy structure was solvated with 12 576 solvent molecules (SPC model) in a cubic solvent box of dimensions (73.2 Å^3). The system was initially minimised using the standard NPT relaxation protocol to reduce the steric clashes. In the first step, the solute was restrained and the solvent was minimised. In the second step, the entire system was minimised without any constraints to a gradient of 0.01 kcal/mole/Å, which yielded the solution structure of *h*GIP.

Modelling the Interaction of *h*GIP with the *N*-terminus of GIPR

The interaction of *h*GIP with the *N*-terminus of GIPR was studied using molecular dynamics simulation. The molecular dynamics simulation studies were carried out using the *Desmond* (v*2.2)* module in the Schrodinger Suite 2009 [24]. The coordinates of the GIP–GIPR *N*-terminal complex were extracted from the protein data bank (PDB code 2QKH). The starting structure for the MD simulation was prepared with the Protein Preparation Wizard of Maestro. The crystal waters were deleted and hydrogen atoms were added to the heavy atom positions of the GIPR *N*-terminus. The solution structure of *h*GIP was anchored to the crystal structure of the *N*-terminal domain of GIPR by superimposition of the backbone atoms of the α-helical region of *h*GIP, i.e. residue Phe6 to residue Ala28, onto the crystal structure; after this the crystal structure of GIP was deleted from the complex to give an initial structure for the MD simulations. The L-type bent at residue Gln29 causes it to project away from the GIPR *N*-terminus and does not experience any steric clashes with the GIPR *N*-terminus. The complex of *h*GIP:*N*-terminal GIPR was solvated with 18 396 SPC waters (Single Point Charge model). Periodic boundary conditions with an orthorhombic box were applied. The solvent in the system was equilibrated with the peptide–protein assembly to reduce the steric clashes using the standard protocol for the relaxation of an NPT *ensemble*. This protocol involves initial minimization of the solvent with the solute restrained followed by complete minimization. The minimization was followed by a set of short simulations of 12–24 ps in sequential NVT and NPT *ensembles* using the Berendsen thermostat and barostat.

The relaxed system was then subjected to a prolonged simulation in six stages. Each stage comprised of a force constraint over the backbone of the peptide–protein complex that was lower than the previous stage. In every stage, the temperature was coupled to a 300-K bath using the Berendsen algorithm [25]. The pressure was isotropically restrained to 1 bar with the Berendsen barostat [25]. High-frequency vibrations were removed by applying the SHAKE algorithm [26] to constrain all bonds to their equilibrium values. Initial velocities were generated randomly from a Maxwell distribution at 300 K in accordance with the masses assigned to the atoms. The trajectories were sampled at intervals of 1.2 ps. To begin with, an 1-ns simulation was run with the backbone of the *h*GIP:*N*-terminal GIPR complex harmonically constrained with a force constant of 100 kcal/mol/Å^2 but with the side chains set free. In the second stage, a decreasing force constant of 50 kcal/mol/Å^2 was applied over the backbone of the lowest energy conformation of *h*GIP:*N*-terminal GIPR complex obtained from the earlier stage. Gradually, decreasing force constants of 25, 10 and 1 kcal/mol/Å^2 were applied in stages 3, 4, and 5, respectively, in each MD simulation that was run for 1 ns. The sixth and final stage was an MD simulation for 1 ns of the lowest energy conformation of *h*GIP:*N*-terminal GIPR complex obtained from the fifth stage without application of any constraints. The canonical *ensemble* obtained from this stage was then analysed by evaluating the interaction energy (van der Waals, Coulombic and total energy) in a residue-wise manner between the peptide and the protein with the *Discover* module of *InsightII v2005L* [22].

Results and Discussion

NMR Structure of *h*GIP

The 1D proton, TOSCY, DQF-COSY and NOESY experiments were used for the identification of the spin systems of individual amino acids. The technique of sequence-specific resonance assignment developed by Wüthrich [27] was used for establishing connectivities between the spin systems. Assignments of the protons of all residues were followed by tracing out the backbone connectivities using the NH_i-αH_i peaks in the TOCSY spectrum and the NH_i-αH_{i-1} peaks in the NOESY spectrum. The fingerprint region of the NOESY spectrum of *h*GIP in 95% H_2O is given

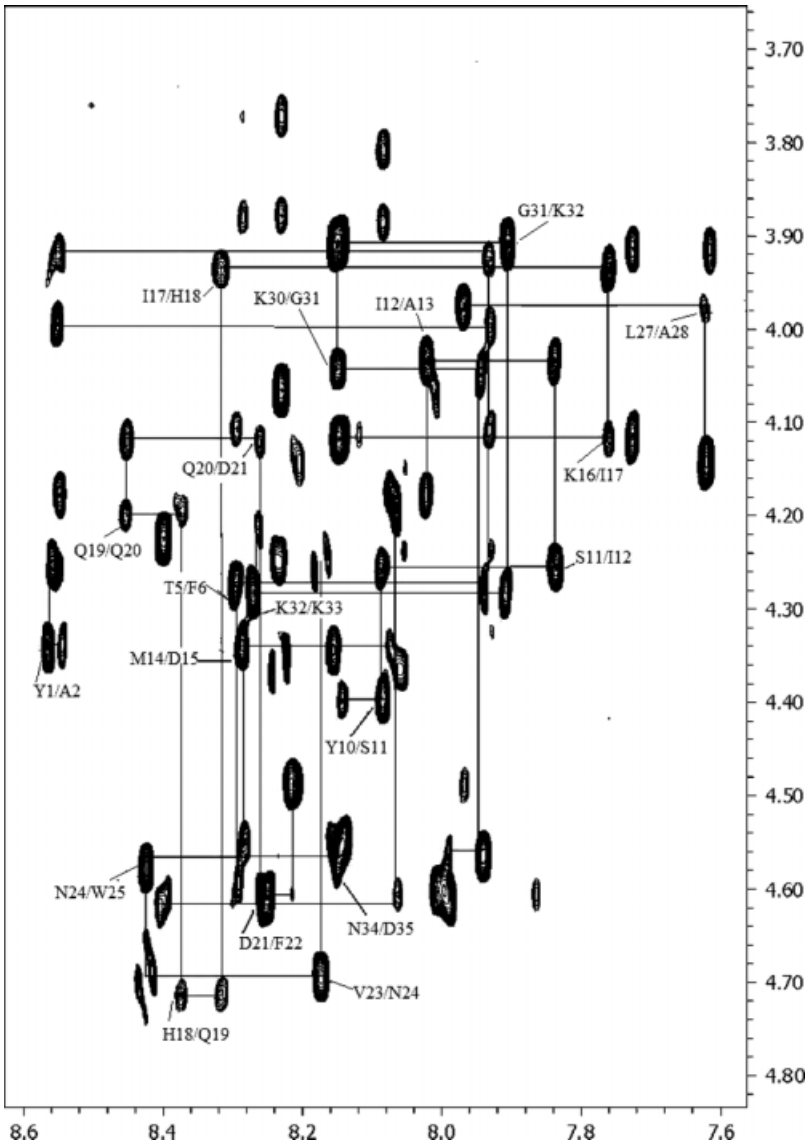

Figure 1. Fingerprint region of the NOESY spectrum (mixing time $\tau_c = 100$ ms) of *h*GIP in H_2O. The backbone 'walk' is shown with some selected connectivities.

in Figure 1. Chemical shifts of methyl resonances were used to identify alanine, leucine and isoleucine residues. The serine residues, Ser8 and Ser11, were identified by their distinctive βH resonances. Non-unique residues were discriminated and other unidentified spin systems identified by direct comparison of the TOCSY and NOESY spectra. Alanine, serine, and threonine residues were used as starting points for the identification of sequence-specific resonance assignments. The connectivities of Tyr1 to Asp15 – except for Glu3 – Lys16 to Gln22 and Gln29 to Asn34 were clearly identified using the $\alpha_i H/N_{i+1}$ and $\beta_i H/N_{i+1}H$ cross peaks in the fingerprint region of the NOESY spectrum. Leu26 to Gln29 connectivities were missing. These residues were assigned using the resonances of Trp25 and Ala28. The different secondary structure motifs show specific patterns of sequential, medium range and long-range NOEs, thereby giving an insight into the 3D structure of the molecule. The presence of $d(\alpha, N)_{i,i+1}$, $d(N, N)_{i,i+2}$, $d(\alpha, N)_{i,i+3}$ and $d(\alpha, N)_{i,i+4}$ connectivities in addition to small $^3J_{NH\alpha}$ coupling constants support an α-helical character of *h*GIP in H_2O. The NOE patterns of *h*GIP in H_2O are given in Figure 2.

The spatial folding of the peptide chains also manifests in the proton and the carbon CSI as a dispersion of the shifts relative to the random coil structure. Helical regions and stretches containing turns are usually characterised by a continuous stretch of negative deviations ('−1') from the random coil values for the αH chemical shift [28] and a positive deviation ('1') in the case of $^{13}C\alpha$ chemical shifts [29]. A β-strand shows exactly an opposite picture. A continuous stretch of '−1' values for the CSI of αH protons of residues Ser8 – Asn39 except Val23 and Gln29 confirms the structured state of *h*GIP. The CSI index for *h*GIP is given in Figure 3.

Temperature coefficients of NH chemical shifts ($-\Delta\delta/\Delta T$) below 3.0 ppb/K and between 3.0 and 5.0 ppb/K indicate that they are shielded from the solvent and suggest that these resonances are in dynamic equilibrium between intramolecularly hydrogen bonded forms and structures with these protons are easily accessible to the solvent. These values for *h*GIP also support the presence of an α-helix [30]. Temperature coefficient values above 5.0 ppb/K, which indicate NH protons freely exposed to the solvent, are seen in the

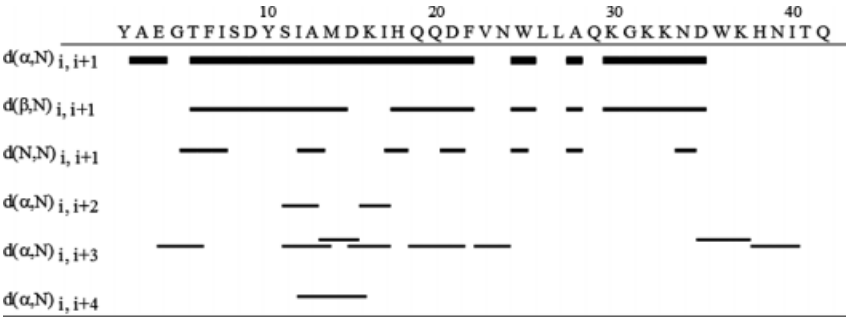

Figure 2. Medium and short range connectivities of *h*GIP in H_2O.

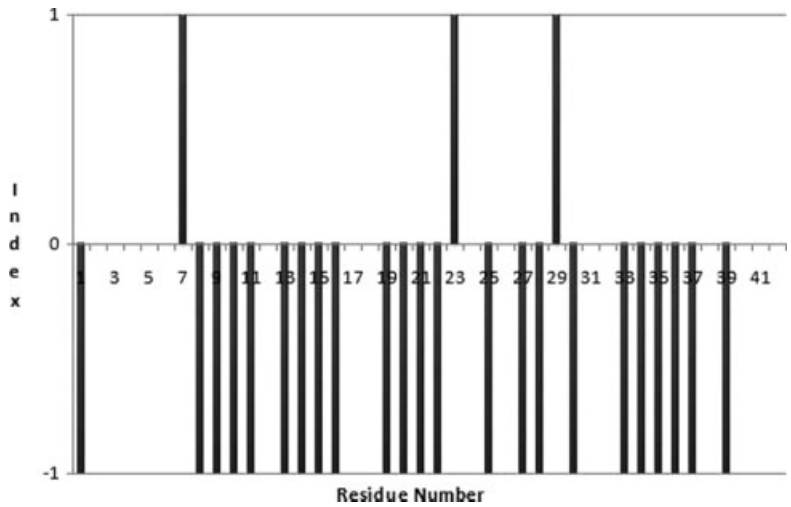

Figure 3. ^{1}H chemical shift index (CSI) for *h*GIP.

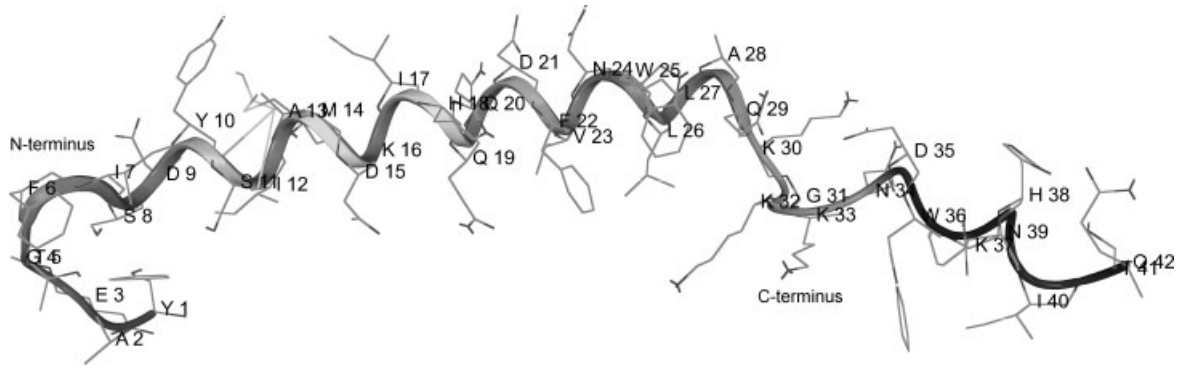

Figure 4. The NMR-derived structure of *h*GIP in H_2O.

amino acids where the α-helix is bent. The structural statistics for the *h*GIP NMR structure are given in Table 1.

The final refined structure of *h*GIP shows a loose α-helical structure between residues Ser8 and Asn39 with some discontinuity at residues Gln29 to Asp35; the helix is bent at Gln29. This bent gives the peptide an 'L' shaped structure (Figure 4). The final structure of *h*GIP deduced by us is in agreement with the literature reports of an α-helical structure of *h*GIP between Ser11 and Gln29 [13,14]. The unbound *h*GIP, like other members of the class B family of GPCR viz. glucagon, parathyroid hormone [31], glucagon-like peptide 1 (GLP-1) [32], exendin-4 [33], pituitary adenylate cyclase activating polypeptide (PACAP) [34], corticotropin-releasing factor (CRF) [35] and others show a limited ordered structure in aqueous solution.

*h*GIP : GIPR *N*-Terminal Interactions

The *ensemble* obtained from the molecular dynamics simulation was analysed to extract key interacting residues and the nature of interactions responsible for binding *h*GIP to the *N*-terminus of GIPR. It is observed that the structure of *h*GIP changes from a loose α-helical one in solution to a tighter α-helical structure upon binding to the *N*-terminus of the GIPR. The exclusively α-helical portion of the *C*-terminus of *h*GIP spanning residues Asp15 to Lys32 is involved in the binding. The α-helix acquires a bend at Gln29 giving an 'L' shaped structure to the α-helix. The base of the L shaped structure does not interact with the *N*-terminus of GIPR and is thus free to interact with other regions of GIPR. The 'L' shape of *h*GIP, seen in the solution structure becomes more pronounced

Table 1. Structural statistics of *h*GIP in 95 : 5 H_2O : D_2O mixture

Total NOE constraints	66
Torsional constraints	17
Temperature coefficients	36
NOE violations >0.2 Å	3
Ramachandran plot regions (%)	
Favoured	85.7
Additionally allowed	9.5
Generously allowed	4.8
Mean atomic RMSD (Å)	
Backbone atoms	3.252
Heavy atoms	3.868
Average energies (kcal/mol)	
Bond stretching	130.3
Angle bending	323.9
Torsional	149.0
van der Waals	−11.2
Total	3040.7

upon binding to the GIPR *N*-terminus. This is seen in the RMSD of 6.63 Å for the two structures, i.e unbound *h*GIP and *h*GIP bound to the *N*-terminus of GIPR. The conformational variation between the bound and unbound forms is represented in Figure 5.

The Coulombic and van der Waals interaction energies of individual residues of *h*GIP that interact with the *N*-terminus of GIPR, over the entire MD trajectory, were classified into three ranges as strong (<−1.0 kcal/mole), moderate (−0.1 to −1 kcal/mole) and weak (>−0.1 kcal/mole) and were used to draw inferences about the intensity of the interactions. Frames were picked at regular intervals from the trajectory to allow sufficient energy variation in the structures to study the interaction pattern.

The *N*-terminus of *h*GIP, i.e. residues Tyr1 to Met14 does not interact with the *N*-terminus of GIPR. A varying pattern of intermolecular hydrogen bonds is observed over the entire trajectory with some hydrogen bonding patterns being consistently observed over the entire trajectory. The *C*-terminal residues Leu26, Leu27 and Gln29 act as hydrogen bond acceptors to $Arg113^R$ (the superscript R denotes residues in the *N*-terminus of GIPR); the hydrogen bonds between these residues are seen regularly in the trajectory including the global minimum structure of the *ensemble*. The mid-terminal residues of *h*GIP such as Asp15 and Lys16 form hydrogen bonds with $Gln30^R$ and $Glu122^R$, respectively, with Asp15 and, Lys16 acting as hydrogen bond donors and $Gln30^R$ and $Glu122^R$ as hydrogen bond acceptors. Structures in the closing stages of the trajectory are attended by hydrogen bonds between Gly31 and Lys32 with $Met67^R$, with the former two residues participating as hydrogen bond donors to $Met67^R$. In addition to hydrogen bonding, a salt bridge is observed between the side chain ε-$^+NH_3$ group of Lys16 in *h*GIP and the side chain carbonyl group of $Glu122^R$ in some frames of the trajectory. The strength of the H-bonds as gauged by the Coulombic energy indicates them to be significant. The hydrogen bonding between residues Asp15 and Gln19 of *h*GIP with $Gln30^R$ seen in the X-ray crystal structure persists in the molecular dynamics trajectory.

Besides hydrogen bonding, the other major interactions observed are hydrophobic and electrostatic interactions (other than H-bond). These interactions were analysed on the global minimum energy structure, and the pattern of variation of the interactions was studied over the entire trajectory. Some important electrostatic interactions are between the backbone carbonyl of $Gln30^R$ or the side chain carbonyl of Asp15 with the side chain NH of Gln19 of *h*GIP; this interaction varies from strong in the initial frames to moderate in the global minima and associated structures and again increases in intensity beyond the structures in the valley of the global minimum. The backbone carbonyl of $Thr31^R$ interacts with the side chain carboxyl OH of Asp15 of *h*GIP strongly in the initial part of the trajectory and then in a moderate manner in the global minimum energy and its associated structures and the rest of the trajectory.

Predominant hydrophobic interactions involve the *h*GIP residues Phe22, Val23, Trp25, Leu26 and Leu27 with the complimentary hydrophobic binding surface of the GIPR *N*-terminal residues $Ala32^R$, $Leu35^R$, $Tyr36^R$, $Trp39^R$, $Met67^R$, $Tyr68^R$, $Tyr87^R$, $Leu88^R$, $Trp90^R$, $Leu111^R$ and $His115^R$. Predominant hydrophobic interactions observed in the X-ray crystal structure are also seen in the molecular dynamics trajectory.

The list of all H-bond, electrostatic and hydrophobic interactions along with their intensities are given in Table 2. Figure 6(a) (ribbon model) and Figure 6(b) (CPK model) show the interactions of *h*GIP with the *N*-terminus of GIPR. Information lacking in the X-ray crystal structure [15] regarding the structural variation of the bound and the unbound form of *h*GIP, the structure of the terminal nine residues (Lys33 to Gln42) of *h*GIP, several elements of the interaction, the dynamics of interactions and the strength

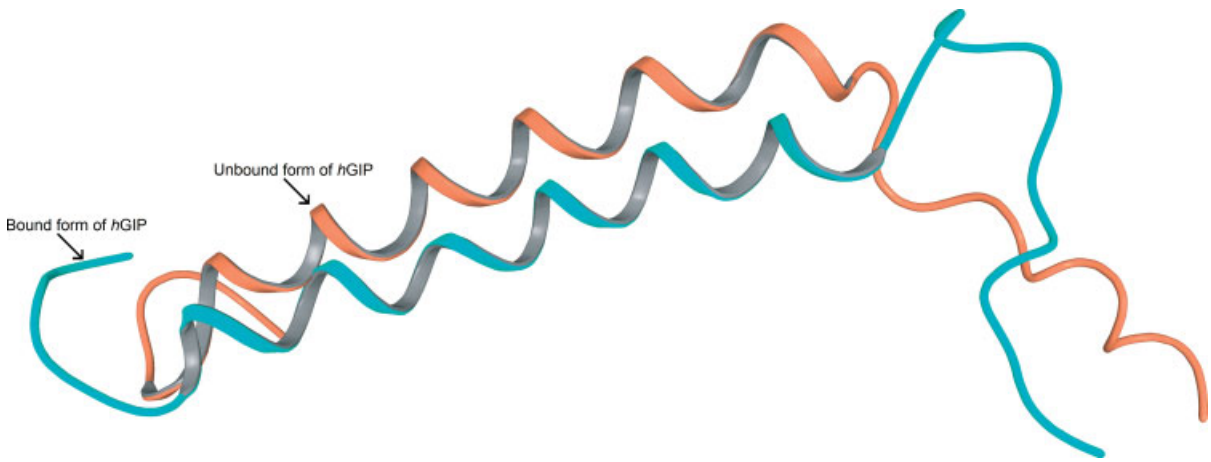

Figure 5. Conformational variation of the bound (cyan) and unbound (orange) forms of *h*GIP.

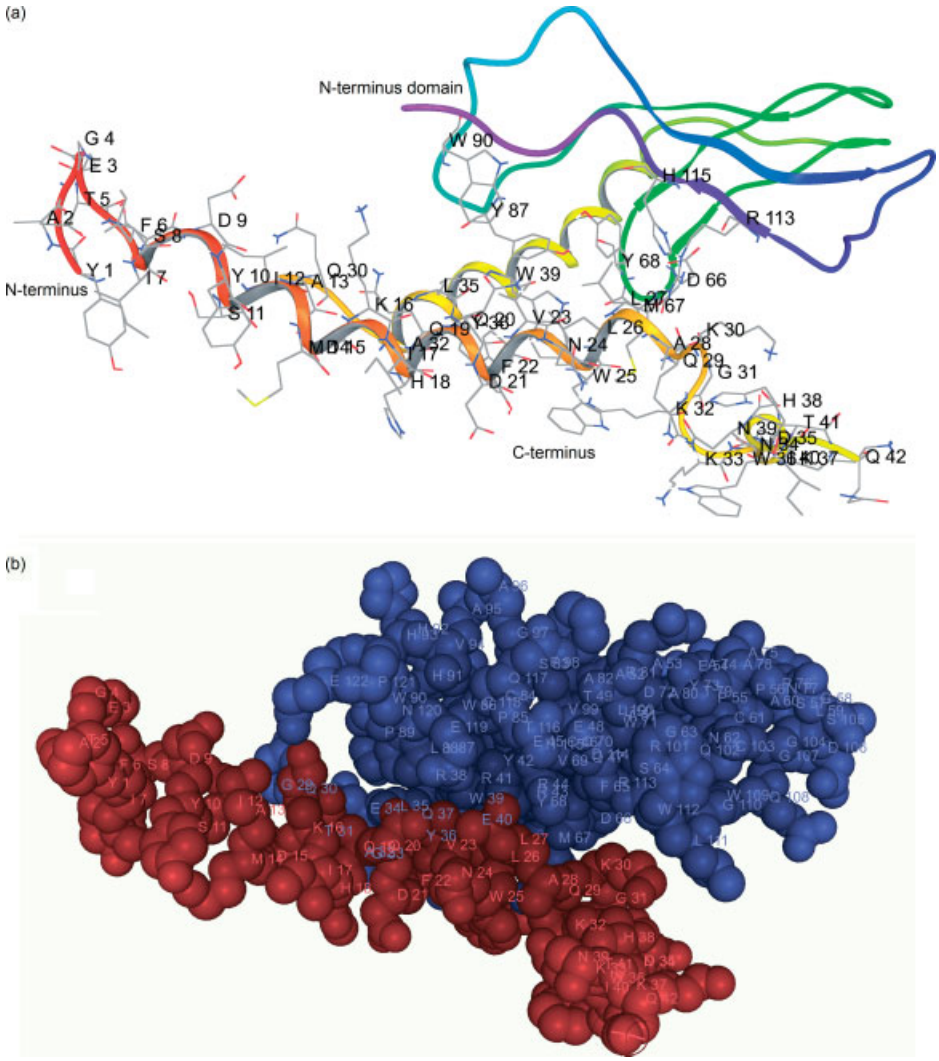

Figure 6. Interaction of *h*GIP with *h*GIPR *N*-terminus seen in the global minimum structure from a MD simulation as depicted by the (a) ribbon and (b) CPK models.

variation of the interaction over the trajectory has been provided by our study.

The missing electron densities of residues 33–42 in the crystal structure could be due to high thermal motions in this segment. This can also be seen in the RMSD values of this segment measured over a 5-ns molecular dynamics trajectory. The RMSD value is 2.947 with a standard deviation of 0.394 for the backbone atoms (Figure 7(a)) and is slightly higher at 3.183 with a standard deviation of 0.290 (Figure 7(b)) for the side chain atoms.

The interaction analysis of *h*GIP with the *N*-terminus of GIPR indicates that the terminal portion of *h*GIP comprising residues 31–42 does not interact at all with the GIPR *N*-terminal domain and is far away from the transmembrane domain to interact with it. From this, we can attribute the equipotency of the full-length GIP(1–42)NH_2 and the truncated peptide GIP(1–30)NH_2 to the lack of involvement of the terminal 12 residues in the interaction with the receptor.

As of date there is no experimentally determined full-length structure of a class B GPCR; however, there are numerous reports of the solution structures of many class B GPCR peptide ligands (unbound state) and the X-ray crystal structure of the extracellular domains (ECDs) of the receptors in complex with their bound peptide ligands. Glucagon [36], parathyroid hormone (PTH) [37], GLP-1, exendin-4, PACAP, CRF and other class B GPCR ligands have been studied in solution as well as co-crystallised with their respective receptor ECDs. *h*GIP and a majority of these peptides all display a limited ordered structure in aqueous solution but adopt a proper tight α-helix upon binding to the ECD of the receptor. This behaviour of *h*GIP like its fellow member ligands reinforces the hypothesis put forth by Parthier *et al*. that activation of class B GPCRs is initiated by an α-helix of the ligand peptide upon binding to the receptor ECD [38].

In conclusion, we have established the complete structure of *h*GIP and have deduced that *h*GIP exhibits a loose α-helical structure between residues Ser8 and Asn39 with some discontinuity from Gln29 to Asp35 and a bend at Gln29 in 95 : 5 H_2O : D_2O mixture. This bend gives *h*GIP an 'L' shaped appearance. The structure of *h*GIP alters to a tight α-helix upon binding to the *N*-terminus of GIPR and the 'L' shaped appearance becomes more pronounced on binding to the receptor. This study has also been able to throw light on the structure of the missing *C*-terminal end (residues Lys33 to Gln42) in the X-ray study. Furthermore, MD simulations of the complex between *h*GIP and the *N*-terminus of GIPR show the important steric, electrostatic

Table 2. *h*GIP–GIPR (*N*-terminus) interactions observed over the molecular dynamics simulation trajectory

*h*GIP residues	GIPR *N*-terminus residues	Nature of interaction	Intensity of interaction
Leu26, Leu27, Gln29	$Arg113^R$	H-bond	Strong
Asp15	$Gln30^R$	H-bond	Strong
Lys16	$Glu122^R$	H-bond	Moderate
Gly31, Lys32	$Met67^R$	H-bond	Moderate
Lys16	$Glu122^R$	Salt bridge	Strong
Asp15	$Gln30^R$	Electrostatic	Strong initially; moderate in the global minima and associated structures and again increases in intensity beyond the global minima region
Asp15	$Thr31^R$	Electrostatic	Strong interaction before and at the global minima region; moderate interactions post global minima region
His18, Gln19, Phe22	$Ala32^R$	Hydrophobic	Moderate
Gln19, Phe22, Val23, Leu26	$Leu35^R$	Hydrophobic	Moderate
Phe22, Trp25, Lys32	$Tyr36^R$	Hydrophobic	Moderate interaction with Phe22 wanes in the later part of the trajectory
Phe22, Trp25, Leu26, Lys32	$Trp39^R$	Hydrophobic	Moderate; strong interaction with Leu26
Lys30	$Asp66^R$	Electrostatic	Strong interaction before and at the global minima region; moderate interactions post global minima region
Leu26, Gln29, Lys30	$Met67^R$	Hydrophobic	Strong
Trp25	$Met67^R$	Hydrophobic	Moderate
Val23, Leu26, Leu27, Lys30	$Tyr68^R$	Hydrophobic	Strong to moderate
Phe22, Val23, Leu26	$Tyr87^R$	Hydrophobic	Moderate
Val23, Leu26	$Leu88^R$	Hydrophobic	Moderate
Gln20, Val23	$Trp90^R$	Hydrophobic	Moderate
lys30	$Arg101^R$, $Leu111^R$	Hydrophobic	Moderate
Leu26, Leu27	$His115^R$	Hydrophobic	Moderate, strong, respectively

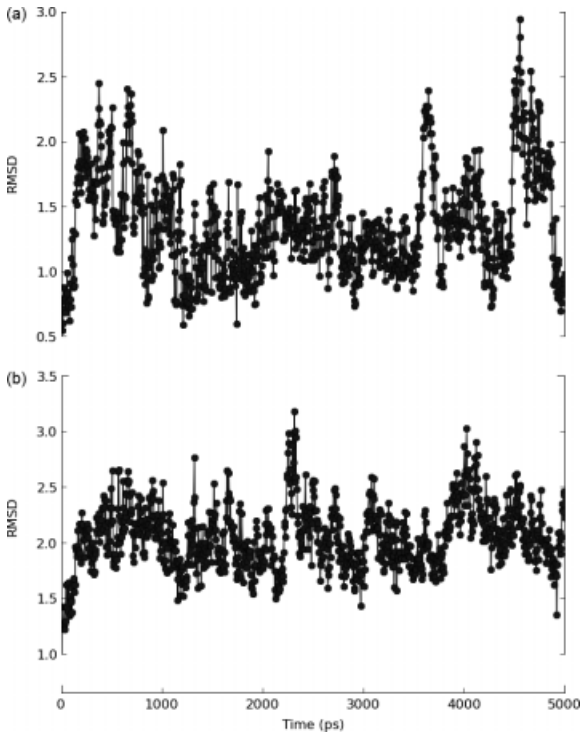

Figure 7. (a) Backbone RMSDs of the 30–42 residue segment of *h*GIP over a 5-ns molecular dynamics trajectory. (b) Side chain RMSDs of the 30–42 residue segment of *h*GIP over a 5-ns molecular dynamics trajectory.

and hydrophobic interactions that evolve with time between the *C*-terminal region – Asp15 to Lys30 of *h*GIP with specific residues in the *N*-terminus of GIPR. This study gives deep insights into the binding pattern and the thermodynamics involved in the binding of GIP to its receptor. This information can be used to design new anti-diabetic molecules.

Acknowledgements

This work was supported by the Department of Science and Technology (DST), New Delhi through grants SR/S0/BB-10/2005. The facilities provided by the National Facility for High Field NMR located at TIFR are greatly acknowledged.

References

1 Jornvall H, Carlquist M, Kwauk S, Otte SC, McIntosh CH, Brown JC, Mutt V. Amino acid sequence and heterogeneity of gastric inhibitory polypeptide (GIP). *FEBS Lett.* 1981; **123**: 205–210.
2 Meier JJ, Nauck MA, Schmidt WE, Gallwitz B. Gastric inhibitory polypeptide: the neglected incretin revisited. *Regul. Pept.* 2002; **107**: 1–13.
3 Lu M, Wheeler MB, Leng XH, Boyd AE, 3rd. The role of the free cytosolic calcium level in beta-cell signal transduction by gastric inhibitory polypeptide and glucagon-like peptide I(7–37). *Endocrinology* 1993; **132**: 94–100.
4 Gault VA, O'Harte FP, Harriott P, Mooney MH, Green BD, Flatt PR. Effects of the novel (Pro3)GIP antagonist and exendin(9–39)amide on GIP- and GLP-1-induced cyclic AMP generation, insulin secretion and postprandial insulin release in obese diabetic (ob/ob) mice:

evidence that GIP is the major physiological incretin. *Diabetologia* 2003; **46**: 222–230.
5 Eckel RH, Fujimoto WY, Brunzell JD. Gastric inhibitory polypeptide enhanced lipoprotein lipase activity in cultured preadipocytes. *Diabetes* 1979; **28**: 1141–1142.
6 Raben A, Andersen HB, Christensen NJ, Madsen J, Holst JJ, Astrup A. Evidence for an abnormal postprandial response to a high-fat meal in women predisposed to obesity. *Am. J. Physiol.* 1994; **267**: E549–E559.
7 Wasada T. Effect of gastric inhibitory polypeptide on plasma levels of chylomicron triglycerides in dogs. *J. Clin. Invest.* 1981; **68**: 1106–1107.
8 Yip RGC, Boylan MO, Kieffer TJ, Wolfe MM. Functional GIP receptors are present on adipocytes. *Endocrinology* 1998; **139**: 4004–4007.
9 Deacon CF, Nauck MA, Meier J, Hucking K, Holst JJ. Degradation of endogenous and exogenous gastric inhibitory polypeptide in healthy and in type 2 diabetic subjects as revealed using a new assay for the intact peptide. *J. Clin. Endocrinol. Metab.* 2000; **85**: 3575–3581.
10 Mentlein R, Gallwitz B, Schmidt WE. Dipeptidyl-peptidase IV hydrolyses gastric inhibitory polypeptide, glucagon-like peptide-1(7–36)amide, peptide histidine methionine and is responsible for their degradation in human serum. *Eur. J. Biochem.* 1993; **214**: 829–835.
11 O'Harte FP, Mooney MH, Flatt PR. NH_2-terminally modified gastric inhibitory polypeptide exhibits amino-peptidase resistance and enhanced antihyperglycemic activity. *Diabetes* 1999; **48**: 758–765.
12 Malde AK, Srivastava SS, Coutinho EC. Understanding interactions of gastric inhibitory polypeptide (GIP) with its G-protein coupled receptor through NMR and molecular modeling. *J. Pept. Sci.* 2007; **13**: 287–300.
13 Alana I, Malthouse JP, O'Harte FP, Hewage CM. The bioactive conformation of glucose-dependent insulinotropic polypeptide by NMR and CD spectroscopy. *Proteins* 2007; **68**: 92–99.
14 Alana I, Parker JC, Gault VA, Flatt PR, O'Harte FP, Malthouse JP, Hewage CM. NMR and alanine scan studies of glucose-dependent insulinotropic polypeptide in water. *J. Biol. Chem.* 2006; **281**: 16370–16376.
15 Parthier C, Kleinschmidt M, Neumann P, Rudolph R, Manhart S, Schlenzig D, Fanghanel J, Rahfeld JU, Demuth HU, Stubbs MT. Crystal structure of the incretin-bound extracellular domain of a G protein-coupled receptor. *Proc. Natl. Acad. Sci. U.S.A.* 2007; **104**: 13942–13947.
16 Derome A, Williamson M. 2D homonuclear shift correlation phase sensitive using TPPI with double quantum filter phase cycle. *J. Magn. Reson.* 1990; **88**: 177–185.
17 Kumar A, Ernst RR, Wüthrich K. A two-dimensional nuclear Overhauser enhancement (2D NOE) experiment for the elucidation of complete proton–proton cross-relaxation networks in biological macromolecules. *Biochem. Biophys. Res. Commun.* 1980; **95**: 1–6.
18 Bax A, Davis DG. MLEV-17 based two-dimensional homonuclear magnetization transfer spectroscopy. *J. Magn. Reson.* 1985; **65**: 355–360.
19 Hwang TL, Shaka AJ. Water suppression that works. Excitation sculpting using arbitrary waveforms and pulsed field gradients. *J. Magn. Reson.* 1995; **112**: 275–279.
20 Wüthrich K. *NMR of Proteins and Nucleic Acids*. John Wiley & Sons: New York, 1986.
21 Vuister GW, Bax A. Quantitative J correlation: a new approach for measuring homonuclear three-bond J(HNH.alpha.) coupling constants in 15N-enriched proteins. *J. Am. Chem. Soc.* 1993; **115**: 7772–7777.
22 *Insight-II*. Accelrys Inc.: San Diego, CA, USA, 2005.
23 Maple JR, Dinur U, Hagler AT. Derivation of force fields for molecular mechanics and dynamics from ab initio energy surfaces. *Proc. Natl. Acad. Sci. U.S.A.* 1988; **85**: 5350–5354.
24 Bowers KJ, Chow E, Xu H, Dror RO, Eastwood MP, Gregersen BA, Klepeis JL, Kolossvary I, Moraes MA, Sacerdoti FD, Salmon JK, Shan Y, Shaw DE. In *Supercomputing, 2006. SC '06. Proceedings of the ACM/IEEE SC 2006 Conference*, 2006, Tampa, FL, 2006; 43.
25 Berendsen HJC, Postma JPM, Gunsteren WFv, DiNola A, Haak JR. Molecular dynamics with coupling to an external bath. *J. Chem. Phys.* 1984; **81**: 3684–3690.
26 Ryckaert J-P, Ciccotti G, Berendsen HJC. Numerical integration of the cartesian equations of motion of a system with constraints: molecular dynamics of n-alkanes. *J. Comput. Phys.* 1977; **23**: 327–341.
27 Wüthrich K, Billeter M, Braun W. Polypeptide secondary structure determination by nuclear magnetic resonance observation of short proton–proton distances. *J. Mol. Biol.* 1984; **180**: 715–740.
28 Wishart DS, Sykes BD, Richards FM. Chemical shift index: a fast and simple method for the assignment of protein secondary structure through NMR spectroscopy. *Biochemistry* 1992; **31**: 1647–1651.
29 Wishart DS, Sykes BD. The 13C chemical-shift index: a simple method for the identification of protein secondary structure using 13C chemical-shift data. *J. Biomol. NMR* 1994; **4**: 171–180.
30 Bach AC, Eyermann CJ, Gross JD, Bower MJ, Harlow RL, Weber PC, DeGrado WF. Structural studies of a family of high affinity ligands for GPIIb/IIIa. *J. Am. Chem. Soc.* 1994; **116**: 3207–3219.
31 Marx UC, Adermann K, Bayer P, Forssmann WG, Rosch P. Solution structures of human parathyroid hormone fragments *h*PTH(1–34) and *h*PTH(1–39) and bovine parathyroid hormone fragment *b*PTH(1–37). *Biochem. Biophys. Res. Commun.* 2000; **267**: 213–220.
32 Thornton K, Gorenstein DG. Structure of glucagon-like peptide (7–36) amide in a dodecylphosphocholine micelle as determined by 2D NMR. *Biochemistry* 1994; **33**: 3532–3539.
33 Neidigh JW, Fesinmeyer RM, Prickett KS, Andersen NH. Exendin-4 and glucagon-like-peptide-1: NMR structural comparisons in the solution and micelle-associated states. *Biochemistry* 2001; **40**: 13188–13200.
34 Sun C, Song D, Davis-Taber RA, Barrett LW, Scott VE, Richardson PL, Pereda-Lopez A, Uchic ME, Solomon LR, Lake MR, Walter KA, Hajduk PJ, Olejniczak ET. Solution structure and mutational analysis of pituitary adenylate cyclase-activating polypeptide binding to the extracellular domain of PAC1-RS. *Proc. Natl. Acad. Sci. U.S.A.* 2007; **104**: 7875–7880.
35 Georgios AS, Spyridon P, George P, Paul C. Monitoring the structural consequences of Phe122→D-Phe192 and Leu15→Aib substitution in human/rat corticotropin releasing hormone. Implications for design of CRH antagonists. *Eur. J. Biochem.* 2002; **269**: 6009–6019.
36 Sasaki K, Dockerill S, Adamiak DA, Tickle IJ, Blundell T. X-ray analysis of glucagon and its relationship to receptor binding. *Nature* 1975; **257**: 751–757.
37 Jin L, Briggs SL, Chandrasekhar S, Chirgadze NY, Clawson DK, Schevitz RW, Smiley DL, Tashjian AH, Zhang F. Crystal structure of human parathyroid hormone 1–34 at 0.9-Å resolution. *J. Biol. Chem.* 2000; **275**: 27238–27244.
38 Parthier C, Reedtz-Runge S, Rudolph R, Stubbs MT. Passing the baton in class B GPCRs: peptide hormone activation via helix induction?. *Trends Biochem. Sci.* 2009; **34**: 303–310.

